Autotrophic and mixotrophic metabolic network fluxes suggest versatile lifestyle for the anammox bacterium *Candidatus* Kuenenia stuttgartiensis

Christopher E. Lawson[1,*], Rob M. de Graaf [2], Guylaine Nuijten[2], Tyler B. Jacobson[3], Martin Pabst[4], David. M. Stevenson[3], Mike S.M. Jetten[2], Daniel R. Noguera[1,5], Katherine D. McMahon[1,3], Daniel Amador-Noguez[3], Sebastian Lücker[2,*]

[1]Department of Civil and Environmental Engineering, University of Wisconsin-Madison, Madison, WI, USA
[2]Department of Microbiology, Institute for Water and Wetland Research, Radboud University, Nijmegen, the Netherlands
[3]Department of Bacteriology, University of Wisconsin-Madison, Madison, WI, USA
[4]Department of Biotechnology, Delft University of Technology, Delft, The Netherlands
[5]DOE Great Lakes Bioenergy Research Center, University of Wisconsin-Madison, Madison, WI, USA

[*]Corresponding authors: Christopher E. Lawson (c.e.lawson.87@gmail.com), Sebastian Lücker (s.luecker@science.ru.nl)

Abstract

Anaerobic ammonium-oxidizing (anammox) bacteria mediate a key step in the biogeochemical nitrogen cycle and have been applied worldwide for the energy-efficient removal of nitrogen from wastewater. However, outside their core energy metabolism, little is known about the metabolic networks driving anammox bacterial anabolism and mixotrophy beyond genome-based predictions. Here, we experimentally resolved the central carbon metabolism of the anammox bacterium *Candidatus* Kuenenia stuttgartiensis using time-series ^{13}C isotope tracing, metabolomics, and isotopically nonstationary metabolic flux analysis (INST-MFA). Our findings confirm predicted metabolic pathways used for CO_2 fixation, central metabolism, and amino acid biosynthesis in *K. stuttgartiensis*, and reveal several instances where genomic predictions are not supported by *in vivo* metabolic fluxes. This includes the use of an incomplete oxidative tricarboxylic acid cycle, despite the genome not encoding a known citrate synthase. We also demonstrate that *K. stuttgartiensis* is able to directly assimilate formate via the Wood-Ljungdahl pathway instead of oxidizing it completetly to CO_2 followed by reassimilation. In contrast, our data suggests that acetate is fully oxidized to CO_2 via reversal of the Wood-Ljungdahl pathway and partial TCA cycle activity, followed by reassimilation of the produced CO_2. Together, these

findings highlight the versatility of central carbon metabolism in anammox bacteria and will enable the construction of accurate metabolic models that predict their function in natural and engineered ecosystems.

Main

Anaerobic ammonium oxidation (anammox) is a key step in the biogeochemical nitrogen cycle and represents a novel treatment process for the sustainable removal of nitrogen from wastewater. The process is mediated by a deeply branching group of chemolithoautotrophic bacteria within the Planctomycetes, the Brocadiales, that couple the anaerobic oxidiation of ammonium to nitrite reduction and dinitrogen gas formation[1,2,3,4]. The discovery of this unique metabolism and subsequent translation to full-scale applications represents one of the most rapid biotechnological advances in wastewater treatment[5,6,7]. However, the metabolic networks controlling anammox metabolism remain poorly understood, which limits the prediction of their function in natural and engineered ecosystems.

Metagenomic sequencing together with experimental studies have begun to unravel the metabolic potential of anammox bacteria[2,3,8]. A combination of molecular approaches have been used to reveal the key enzymes and reactions involved in anammox catabolism, which include hydrazine (N_2H_4) and nitric oxide (NO) as volatile intermediates in the anammox bacterium *Candidatus* Kuenenia stuttgartiensis (hereafter, *K. stuttgartiensis*)[3,9,10]. These reactions are localized within a specialized intracellular organelle, the anammoxosome, which is believed to be dedicated to energy conservation[11,12] and also contains membrane-bound respiratory complexes of *K. stuttgartiensis*' electron transport chain, including complex I, ATP synthase, and an NAD+:ferredoxin oxidoreductase (RNF)[13]. Experimental studies together with genomic evidence have also suggested that anammox bacteria are much more versatile than initially assumed, and can use alternative electron donors to ammonium, such as formate, acetate, and propionate for energy conservation with nitrite or nitrate as electron acceptors[2,8,14,15,16,17]. Intriguingly, it has been proposed that these organic substrates are fully oxidized to CO_2 and not directly assimilated into cell biomass, suggesting that anammox bacteria adhere to their autotrophic lifestyle[4].

Based on measurements of cell carbon isotopic composition, genomic evidence, and gene expression data, it has been proposed that anammox bacteria fix CO_2 to acetyl-CoA via the Wood-Ljungdahl pathway[2,4,18,19]. Four additional carboxylation reactions are also predicted to

incorporate CO_2 into central carbon metabolism based on *K. stuttgartiensis'* genome annotations, catalyzed by pyruvate:ferredoxin oxidoreductase (PFOR), 2-oxoglutarate:ferredoxin oxidoreductase (OFOR), pyruvate carboxylase, and phosphoenolpyruvate carboxylase[2,4]. Products from these reactions are proposed to flow through the tricarboxylic acid (TCA) cycle, gluconeogenesis, and the pentose phosphate pathway to synthesize all biomass precursor metabolites[2,4]. Since *K. stuttgartiensis* apparently lacks a citrate synthase gene, it has been hypothesized that the TCA cycle operates in the reductive direction via OFOR to synthesize essential precursor metabolites, such as alpha-ketoglutarate[4]. However, these genome-based predictions of *K. stuttgartiensis'* metabolic network remain to be tested.

Here, we experimentally resolved the central carbon metabolism of a planktonic *K. stuttgartiensis* cell culture (more than 95% enriched) using time-series ^{13}C isotope tracing, metabolomics, and isotopically nonstationary metabolic flux analysis (INST-MFA). Our results show that several of the metabolic predictions summarized above, which were primarily based on genomic evidence, are not supported by the flux of metabolites experimentally observed. For instance, *K. stuttgartiensis* operates an incomplete oxidative TCA cycle despite having no predicted citrate synthase gene. We also demonstrate that *K. stuttgartiensis* is able to directly assimilate formate via the Wood-Ljungdahl pathway instead of oxidizing it to CO_2 before assimilation. On the contrary, we show that acetate is fully oxidized to CO_2 via a reversed Wood-Ljungdahl pathway and a partial TCA cycle, followed by reassimilation of the produced CO_2. These findings highlight the versatility of carbon metabolism in *K. stuttgartiensis* and provide fundamental insights on the metabolic networks controlling anammox bacterial anabolism.

Results

Mapping anammox autotrophic metabolism. To elucidate the central carbon metabolic network of *K. stuttgartiensis* under chemolithoautotrophic growth conditions, we first performed time-series isotopic tracer experiments with ^{13}C-bicarbonate coupled to metabolomic analysis. Planktonic *K. stuttgartiensis* cells were cultivated under steady-state conditions in a continuous-flow membrane bioreactor using minimal media supplemented with ammonium and nitrite. Subsequently, ^{13}C-labelled bicarbonate was rapidly introduced into the bioreactor to a concentration of 30 mM (approximately 65% ^{13}C-dissolved inorganic carbon, DIC), which

incorporated into *K. stuttgartiensis*' metabolome over time. Samples were collected over a 3-hour period to trace metabolic network structure based on rates of metabolite ^{13}C-enrichment.

Based on proposed carbon assimilation pathways for anammox bacteria[2,4], we expected that CO_2 fixation would largely occur through the Wood-Ljungdahl pathway and PFOR, resulting in fast labelling of acetyl-CoA and pyruvate, followed by phosphoenolpyruvate and other downstream metabolites. However, despite the almost immediate labeling of phosphoenolpyruvate, ^{13}C-enrichment of acetyl-CoA and pyruvate was slow during the 3-hour experiment (Figure 1a; Figure 1b). One hypothesis for this observation is substrate channeling, where the product of one enzymatic reaction is directly passed to the next enzyme without opportunity to equilibrate within the cytoplasm[20]. Substrate channeling has been previously reported as a mechanism to protect highly labile intermediates of the Wood-Ljungdahl pathway[21,22] or regulate acetyl-CoA biosynthesis[23], and in *K. stuttgartiensis* it could be combined with PFOR to form a channel from CO_2 to phosphoenolpyruvate. An alternative explanation could be that different pools of acetyl-CoA and pyruvate exist through compartmentation. For example, the Wood-Ljungdahl pathway and PFOR activities could occur in one compartment or specific cytoplasmic location[24], where other pools of acetyl-CoA and pyruvate that do not get labelled exist in another, diluting the overall ^{13}C metabolite measurements. Consistent with the latter, amino acids synthesized from pyruvate (i.e., valine, and alanine) showed faster labelling and higher ^{13}C-enrichment (Figure 1a; Figure 1b).

Acetyl-CoA and pyruvate are expected to enter the TCA cycle and gluconeogenesis to produce biomass precursors. Since *K. stuttgartiensis'* genome does not encode a citrate synthase required to operate the oxidative TCA cycle, it is hypothesized that synthesis of key precursor metabolites, including succinyl-CoA and alpha-ketoglutarate, occurs via the reductive direction[4]. If this hypothesis is correct, we would expect to observe high ^{13}C-labelling of oxaloacetate, succinate, and alpha-ketoglutarate. While fast labeling of aspartic acid, which was used as a surrogate for oxaloacetate labelling, implied high activity of phosphoenolpyruvate (or pyruvate) carboxylase, ^{13}C-labelling of succinate was much less and slower than the labelling of alpha-ketoglutarate (Figure 1b; Figure 1c). This suggested that OFOR and other reductive TCA cycle enzymes were not operating in *K. stuttgartiensis* to synthesize alpha-ketoglutarate.

Other biomass precursors are additionally predicted to be synthesized from gluconeogenesis and the pentose phosphate pathway in *K. stuttgartiensis*[2]. Consistent with this,

we observed fast ^{13}C-labeling of the gluconeogenic intermediates 3-phosphoglycerate, fructose 6-phosphate, and glucose 6-phosphate, as well as pentose phosphate pathway intermediates, such as sedheptulose 7-phosphate and ribose 5-phosphate (Figure 1b; Figure 1c; Supplementary Dataset 1).

^{13}C-formate tracing confirms formate assimilation pathways and oxidative TCA cycle in *K. stuttgartiensis*. We further probed central carbon metabolism with ^{13}C-formate. While it has been proposed that anammox bacteria fully oxidize organic substrates, such as formate, to CO_2[4], we hypothesized that formate could be assimilated by *K. stuttgartiensis* via the methyl branch of the Wood-Ljundahl pathway. This would result in a positionally labelled acetyl-CoA pool that would provide additional information on metabolic network activity (Figure 2a).

We tested this hypothesis by rapidly introducing ^{13}C-formate into fresh continuous cultures of *K. stuttgartiensis* to a concentration of 50 mM followed by metabolome sampling over 180 minutes (14 timepoints total). Within 1.5 minutes of ^{13}C-formate introduction, we observed steady-state labelling of several central metabolites, including phosphoenolpyruvate (Figure 2b) and 3-phosphoglycerate (Figure 3b), consistent with direct assimilation of formate. In agreement with formate assimilation via the Wood-Ljungdahl pathway, only the M+1 mass isotopomer of acetyl-CoA became enriched during the experiment (Figure 2c). M+1 mass isotopomers of phosphoenolpyruvate and aspartic acid (oxaloacetate surrogate) were also dominant (Figure 2c), consistent with their synthesis from acetyl-CoA via the sequential reactions of PFOR, phosphoenolpyruvate synthase, and phosphoenolpyruvate (or pyruvate) carboxylase, respectively. Since only a very minor fraction of the M+2 mass isotopomer were detected in these metabolites (<3% over initial 45 minutes), it can be concluded that intracellular ^{13}C-CO_2 concentrations remained low during the experiment. Consistent with this, measured ^{13}C-DIC content in the liquid media produced from ^{13}C-formate oxidation was low, increasing to only 5% over 45 minutes (Figure 2b). This supports the inference that ^{13}C-inorganic carbon incorporation into metabolites was insignificant compared to the rate of incorporation via ^{13}C-formate. Similar to ^{13}C-bicarbonate experiments, slower labelling of acetyl-CoA and pyruvate was observed during the ^{13}C-formate tracer experiments (Figure 2b; Figure 2c). This further supports the hypothesis that separate intracellular pools of these metabolites may exist in *K. stuttgartiensis*.

^{13}C-formate labelling experiments also allowed us to analyze operation of the TCA cycle. If the reductive TCA cycle was operating in *K. stuttgartiensis* only a single carbon in alpha-ketoglutarate would be labelled (from oxaloacetate), while two carbons would be labelled if alpha-ketoglutarate was produced oxidatively (from oxaloacetate and acetyl-CoA). Consistent with the latter route, mass isotopomer distributions for citrate and alpha-ketoglutarate consisted largely of M+2 mass isotopomers (Figure 2c). This clearly demonstrates that alpha-ketoglutarate was produced via an oxidative TCA cycle in *K. stuttgartiensis*, and not via the reductive TCA cycle. On the contrary, malate, fumarate, and succinate pools were largely comprised of M+1 mass isotopomers (Figure 2c), which suggests that a bifurcated TCA cycle was operating.

The labelling patterns of TCA cycle metabolites suggest that *K. stuttgartiensis* uses a novel or highly divergent enzyme for citrate synthesis. While no citrate synthase is annotated in the *K. stuttgartiensis* genome, several acyltransferase candidates exist, including genes annotated as (R)-citramalate synthase (KSMBR1_RS19040) believed to be involved in isoleucine biosynthesis[25] and redundant copies of 2-isopropylmalate synthase (KSMBR1_RS18315 and KSMBR1_RS10820). In particular, one of the 2-isopropylmalate synthase genes (KSMBR1_RS10820) is phylogenetically related (55.1% identity) to *Re*-citrate synthase identified in *Clostridium kluyveri*[26] and is located next to an ADP-forming succinate-CoA ligase of the oxidative TCA cycle. Therefore, we posit that this gene encodes a dedicated *Re*-citrate synthase that allows the oxidative TCA cycle to be operational in *K. stuttgartiensis*.

Multiple pathways for sugar phosphate biosynthesis? Results from the ^{13}C-formate tracer experiments also allowed for closer examination of pentose and hexose sugar phosphate biosynthesis in *K. stuttgartiensis.* Because the labelled pools of 3-phosphoglycerate and dihydroxyacetone phosphate were largely comprised of M+1 mass isotopomers, we expected fructose 6-phosphate to largely consist of M+2 mass isotopomers based on gluconeogenesis reactions (Figure 3a). However, a considerable fraction of fructose 6-phosphate (Figure 3b) and glucose 6-phosphate (Supplementary Dataset 1) were consistently present as M+1 mass isotopomers during the ^{13}C-formate tracer experiment (~25-45%). While it is possible that this labeling pattern was produced during the period when the M+1 isotopomers of dihydroxyacetone phosphate and glyceraldehyde 3-phosphate were ~50% (<1.5 minutes), it more likely suggests that alternative pathways exist for sugar phosphate biosynthesis in *K. stuttgartiensis*.

Amino acid biosynthetic pathways. ^{13}C-formate tracer results were also used to confirm major amino acid biosynthetic pathways in *K. stuttgartiensis*. Our data supports the synthesis of aspartate, asparagine, and threonine via canonical routes from oxaloacetate; the synthesis of glutamate glutamine, proline, and arginine from alpha-ketogluturate; and the synthesis of serine from 3-phosphoglycerate (Supplementary Figure 1). Labelling patterns for valine, alanine, and leucine support their production via canonical branched chain amino acid biosynthesis pathways from pyruvate (Supplementary Figure 1). Interestingly, isoleucine biosynthesis was not supported by canonical routes from threonine, but rather via a recently described citramalate-dependent pathway from acetyl-CoA and pyruvate[27,28] (Supplementary Figure 1). Finally, labeling patterns supported the synthesis of the aromatic amino acids, phenylalanine and tyrosine from erythrose 4-phosphate and phosphoenolpyruvate via the shikimate pathway (Supplementary Figure 1). These amino acid biosynthetic pathways were consistent with pathways predicted from the *K. stuttgartiensis* genome annotation.

Despite the *K. stuttgartiensis* genome lacking an annotated pathway for methionine biosynthesis, methionine was labelled during both ^{13}C-formate and ^{13}C-bicarbonate experiments. Canonical precursors for methionine biosynthesis include aspartic acid and methyl-THF (from formate via methyl-branch of Wood Ljungdahl pathway), thus if this pathway were operating, we would expect to see mainly M+2 methionine. However, a considerable pool of M+1 methionine was consistently observed in our experiments (Supplementary Figure 1), suggesting that a potentially novel pathway is operating to synthesize methionine in *K. stuttgartiensis* that remains to be elucidated.

Acetate oxidation pathway of anammox bacteria. In addition to formate, we also examined the impact of acetate on *K. stuttgartiensis*' metabolic network. While it has been proposed that anammox bacteria can oxidize acetate to CO_2[8,29], the pathways used for acetate oxidation and whether or not acetate is assimilated into biomass have yet to be resolved. If acetate were oxidized to CO_2, we expected that it would initially be incorporated into acetyl-CoA based on previous enzymatic studies with AMP-forming acetyl-CoA synthetase (KSMBR1_RS14485)[30], followed by oxidation to CO_2 via either the oxidative TCA cycle or reversal of the Wood-Ljungdahl

pathway, as previously suggested for other anaerobic chemolithoautotrophic bacteria[31,32] (Figure 4a).

To elucidate metabolic pathways involved in acetate metabolism, we rapidly introduced [2-^{13}C]acetate into active continuous cultures of *K. stuttgartiensis* to a final concentration of 10 mM and sampled the metabolome over 180 minutes (12 timepoints). Within 1.5 minutes after [2-^{13}C]acetate addition, we observed steady-state enrichment of the M+1 mass isotopomer of acetyl-CoA, indicating its synthesis via CoA acetylation (Figure 4c). Considerable ^{13}C-labelling of citrate and glutamate was also observed, suggesting partial oxidative TCA cycle activity (Figure 4c). However, the mass isotopomer distributions for citrate and glutamate contained heavier mass isotopomers (up to M+4) and appeared more evenly distributed, an observation more consistent with the labeling patterns observed during ^{13}C-bicarbonate tracing (Figure 1c) versus ^{13}C-formate tracing (Figure 2c). This pattern can be explained by additional acetate oxidation via the reverse Wood-Ljungdahl pathway to ^{13}C-CO_2, followed by reincorporation of ^{13}C-CO_2 into central metabolites. In agreement with this, mass isotopomer distributions for all other measured metabolites, including phosphoenolpyruvate, 3-phosphoglycerate, dihydroxyacetone phosphate, and fructose 6-phosphate, had relatively even distributions of ^{13}C-labelled mass isotopomers, suggesting they were also synthesized from re-incorporated ^{13}C-CO_2 (Figure 4c). Since ^{13}C-enrichment for most of these metabolites were approximately 2-10 times higher than that of ^{13}C-CO_2 in the media (Figure 4b), we conclude that ^{13}C-CO_2 re-incorporation was faster than the efflux of ^{13}C-CO_2.

Surprisingly, metabolites that labelled rapidly during ^{13}C-bicarbonate and ^{13}C-formate experiments, including phosphoenolpyruvate and 3-phosphoglycerate, labelled slowly with ^{13}C-acetate (Figure 4c). This could be additional evidence that spatial separation of carbon metabolism occurs in *K. stuttgartiensis*, contributing to different pools of acetyl-CoA and pyruvate. Separation of the AMP-forming acetyl-CoA synthetase and potentially other central metabolism enzymes to the outer membrane and periplasm has been reported in the chemolithoautotrophic archeon *Ignicoccus hospitalis*[33]. Interestingly, this enzymes shares homology with the AMP-forming acetyl-CoA synthetase found in *K. stuttgartiensis*[30] and both organisms have ATPases localized to their outer membranes (van Niftrik, 2010, PNAS, 2010). While this raises the possibility that similar spatial separation of metabolism may be present in *K. stuttgartiensis,* further experimental validation is required.

^{13}C protein stable isotope probing confirms substrate uptake by *K. stuttgartiensis*. To confirm uptake of labelled substrates into the biomass of *K. stuttgartiensis* cells, we performed shotgun proteomics on peptides extracted from bioreactor cell pellets collected during ^{13}C-labelling experiments. Metaproteomic analysis of samples collected after 0 and 72 hours confirmed that ^{13}C-bicarbonate was incorporated into the *K. stuttgartiensis* proteome, increasing at a median relative isotope abundance of ~50%, consistent with the ^{13}C-DIC content of the liquid media (Supplementary Figure 2). Incorporation of ^{13}C-formate and [2-^{13}C]acetate into the *K. stuttgartiensis* proteome was also detected after 72 hours at median relative isotope abundances of ~30% and ~10%, respectively (Supplementary Figure 2). These values are consistent with the use of the Wood-Ljungdahl pathway for formate assimilation, and with re-assimilation of ^{13}C-CO_2 produced from acetate oxidation, as the ^{13}C-DIC in the liquid media held at ~11% between 5 and 72 hours (Figure 4b).

Isotopically non-stationary metabolic flux analysis of autotrophic growth. To quantitatively examine *K. stuttgartiensis*' central carbon metabolism and obtain intracellular flux measurements, we performed INST-MFA by fitting measured, time-resolved metabolite mass isotopomer distributions from ^{13}C-formate tracer experiments to an isotopomer network model[34]. This provided a quantitative systems-level flux map of *K. stuttgartiensis'* inferred central carbon metabolism (Figure 5). Flux values were normalized to a net CO_2 uptake rate, which was estimated from the growth rate and cell carbon content: 0.0042 hrs^{-1} x 45 mmol-C/gDW = 0.186 mmol-C/gDW/hr. The resulting flux map reproduces the high intracellular flux anticipated through the Wood-Ljungdahl pathway, PFOR, and phosphoenolpyruvate (or pyruvate) carboxylase, which are the main CO_2 fixation reactions that we observed in *K. stuttgartiensis* (Figure 5). INST-MFA also supported alpha-ketoglutarate production via the oxidative TCA cycle. Moreover, instead of running a bifurcated TCA cycle, the INST-MFA analysis predicts that the M+1 isotopomers of fumarate, succinate, and malate were indirectly derived from aspartic acid as a result of histidine and arginine biosynthesis (Figure 5). This suggests that the TCA cycle in *K. stuttgartiensis* operates incompletely, essentially functioning to produce alpha-ketoglutarate (amino acid precursor) and recycle intermediates of amino acid biosynthesis. Considerable oxidative pentose

phosphate pathway flux was also measured (Figure 5). As no transhydrogenase could be identified in the genome, it is likely that this pathway is key for NAPDH generation in *K. stuttgartiensis.*

INST-MFA also allowed us to query alternative reactions for the unexpected labelling patterns of sugar phosphates during ^{13}C-formate tracer experiments. The genome annotation of *K. stuttgartiensis* has genes coding for hexulose 6-phosphate synthase and 6-phospho-3-hexuloisomerase (KSMBR1_RS05220 and KSMBR1_RS18790, respectively). These are key enzymes of the ribulose monophosphate (RuMP) pathway, a formaldehyde assimilation pathway in many methylotrophic bacteria[35]. Together, these reactions fix formaldehyde to fructose 6-phosphate via a hexulose 6-phosphate intermediate[35]. We hypothesize that these reactions, as well as an unidentified formaldehyde dehydrogenase, could explain the considerable M+1 pentose and hexose phosphate isotopomers observed during ^{13}C-formate labelling (Supplementary Figure 3). Including these reactions in our INST-MFA improved the models fit by approximately 19% (SSR of 802.1 versus 988.7, 95% confidence interval), accounting for approximately 23% of the flux synthesizing fructose 6-phosphate (Figure 5).

Discussion

Elucidating the *in vivo* metabolic network of *K. stuttgartiensis* represents a major advance towards predicting the function of anammox bacteria in natural and engineered ecosystems. Our study offers the first measurements of metabolic flux via INST-MFA in a chemolithoautotrophic organism, providing a systems-level flux map for *K. stuttgartiensis* that can be used to understand anammox bacterial central carbon metabolism. The discovery of an incomplete oxidative TCA cycle operating in *K. stuttgartiensis*, likely mediated by a novel *Re*-citrate synthase, avoids the energetically costly use of reduced ferredoxin for alpha-ketoglutarate biosynthesis via the reductive TCA cycle. Furthermore, the considerable flux measured through the oxidative pentose phosphate pathway highlights an important link between carbon and energy metabolism for generating reducing equivalents (i.e. NADPH) in anammox bacteria. Our analysis validated the use of the Wood-Ljungdahl pathway, PFOR, and phosphoenolpyruvate/pyruvate carboxylase for CO_2 fixation in *K. stuttgartiensis* and provided first evidence of possible compartmentalization and/or metabolic channeling in these pathways. This may enable faster pathway kinetics, avoid degradation of unstable tetrahydrofolate-based intermediates, or limit competition between competing reactions, as has been shown with other pathways[36,37].

We also elucidated the role of the Wood-Ljungdahl pathway for formate assimilation by *K. stuttgartiensis* and show that reversal of this pathway can additionally be used for acetate oxidation. This may further support the metabolism of *K. stuttgartiensis* in their anaerobic habitats, where these compounds likely exist as fermentation products[38,39]. Together, these findings provide insight into the mechanisms underlying the observed versatility of anammox bacteria[40] and may inform strategies to control anammox-based bioprocesses via organic substrate addition[41].

Our elucidation of *K. stuttgartiensis' in vivo* metabolic network fluxes will spur further quantitative studies on anammox metabolism and enable the construction of accurate genome-scale metabolic models to predict anammox bacterial physiology. We believe that when integrated with metabolic models of other nitrogen cycling bacteria[42], drastic improvements in the prediction and control of anammox-based biotechnologies and biogeochemical processes will be possible.

Materials and Methods

Cultivation of K. stuttgartiensis cells

A high enrichment of planktonic *K. stuttgartiensis* cells were cultivated in a continuous flow membrane bioreactor (MBR) on mineral salts medium[43] supplemented with 45 mM of both ammonium and nitrite. Cultures were maintained under steady-state conditions at an OD_{600} of 1.0-1.1 via continuous biomass removal and the bioreactor was continuously sparged with Ar/CO_2 (95%/5% v/v) at a rate of 10 ml/min to maintain anaerobic conditions. The reactor hydraulic and solids retention times were approximately 46 hours and 10.5 days, respectively. The temperature and pH of the reactor were controlled at 30°C and 7.3 using a heat exchanger and 1 M $KHCO_3$ buffer, respectively. The reactor was continuously stirred at 600 rpm. Nitrite concentrations were checked daily to ensure nitrite-limited conditions (Nitrite test strips MQuant®, Merck, Darmstadt, Germany).

^{13}C isotope tracer experiments

Isotope tracing experiments with ^{13}C-labelled substrates ([^{13}C]sodium bicarbonate, [2-^{13}C]sodium acetate, and [^{13}C]sodium formate; Cambridge Isotopes Laboratories, MA, USA) were performed separately on continuous cultures of *K. stuttgartiensis* cells harvested from the MBR system. ^{13}C-labelled substrates were rapidly introduced (within 1 minute) into the bioreactor containing *K. stuttgartiensis* cells growing under steady-state conditions. Initial reactor concentrations of

bicarbonate, acetate and formate were approximately 30 mM, 5 mM and 50 mM respectively. Following ^{13}C-label introduction, 5 ml samples were rapidly withdrawn from the reactor at timepoints 0, 1.5, 3, 5, 8, 11, 15, 20, 30, 45, 60, 90, 120, and 180 minutes. Samples were immediately filtered (Millipore 0.45 µm hydrophilic nylon filter HNWPO4700) using a vacuum pump to remove the medium, and filters were placed face down in 1.5 ml of -80ºC extraction solvent (40:40:20 acetonitrile:methanol:water) for cell quenching and metabolite extraction. Samples were then centrifuged (10,000 rpm, 4°C, 5 mins) and 1 ml of cell-free supernatant was collected and stored at -80°C for metabolomic analysis. The time 0 min sample corresponded to the period directly before ^{13}C-label addition. The ratio of $^{13}C/^{12}C$ DIC remained constant during the course of the experiment as determined by gas chromatography coupled with mass spectrometry (GC-MS) analysis (See method below).

Metabolomic analysis

Samples were analysed using a high-performance HPLC–MS system consisting of a Vanquish™ UHPLC system (Thermo Scientific) coupled by electrospray ionization (ESI; negative polarity) to a hybrid quadrupole high-resolution mass spectrometer (Q Exactive Orbitrap, Thermo Scientific) operated in full scan mode for detection of targeted compounds based on their accurate masses. Properties of Full MS–SIM included a resolution of 140,000, AGC target of 1E6, maximum IT of 40 ms and scan range from 70 to 1,000 m/z. LC separation was achieved using an ACQUITY UPLC BEH C18 column (2.1 × 100 mm column, 1.7 µm particle size; part no. 186002352; serial no. 02623521115711, Waters). Solvent A was 97:3 water:methanol with 10 mM tributylamine (TBA) adjusted to pH 8.1–8.2 with 9 mM acetic acid. Solvent B was 100% methanol. Total run time was 25 min with the following gradient: 0 min, 5% B; 2.5 min, 5% B; 5 min, 20% B; 7.5 min, 20% B; 13 min, 55% B; 15.5 min, 95% B; 18.5 min, 95% B; 19 min, 5% B; 25 min, 5% B. Flow rate was 200 µl min^{-1}. The autosampler and column temperatures were 4°C and 25°C, respectively. Mass isotopomer distributions were corrected for natural abundance using the method of Su et al (2017)[44] and ^{13}C enrichment values were calculated using the formula $(1/N)\ \sum_{i=1}^{N} Mi\ \times\ i$, where N is the number of carbon atoms in the metabolite and Mi is the fractional abundance of the ith mass isotopomer.

To improve separation and measurement sensitivity of specific central carbon metabolites and intracellular amino acids, samples were first derivatized with either aniline[45,46] or benzyl

chloroformate[47], respectively. For aniline derivatization, samples were resuspended in 50 µl HPLC-grade water, 5 µl aniline (6M, pH 4.5), and 5 µl N-(3-dimethylaminopropyl)-N'-ethylcarbodiimide hydrochloride, EDC, (200 mg/ml). After 2 hours of incubation at room temperature, 1 ul of triethylamine was added to stop the reaction. For benzl chloroformate derivatization, samples were resuspended in 10 µl HPLC-grade water, 40 µl methanol, 5 µl of triethylamine, and 1 µl benzyl chloroformate and incubated at room temperature for 30 minutes.

GC-MS analysis of dissolved inorganic carbon isotopic fractions

Isotopic fractions of DIC in the liquid media were measured based on a modified headspace method[48]. 3 ml of liquid culture were collected from the bioreactor with a syringe and directly filtered through a sterile 0.45 µm filter (Whatmann, celluloacetate) and 26G needle into a 120 ml bottle containing 1 ml 6M HCl and crimp sealed with a rubber stopper. Prior to adding the liquid sample, bottles and HCl were flushed with either 100% N_2 or Ar gas to void the headspace of background CO_2. Samples were equilibrated with the acid in the bottles for at least 1 hour at room temperature to drive all DIC into the gas phase. 50 µl of the bottles headspace was then injected with a gas tight syringe (Hamilton) into a gas chromatograph (Agilent 6890 equipped with 6 ft Porapak Q columns) at 80°C with helium as a carrier gas at a flow rate of 24 ml/min, coupled to a mass spectrometer (Agilent 5975C MSD; Agilent, Santa Clara, CA) to determine the isotopic fractions of $^{12}CO_2$ and $^{13}CO_2$.

Isotopic non-stationary metabolic flux analysis

Intracellular metabolic fluxes were estimated from the measured metabolite isotope labelling dynamics via INST-MFA using the elementary metabolite unit method[34] implemented in the INCA software package v1.8[49]. Metabolic fluxes and pool sizes were estimated by minimizing the lack-of-fit between measured and computationally simulated metabolite mass isotopomer distributions using least-squares regression. All metabolite mass isotopomer distribution measurements and model reactions used for flux determination are provided in Supplementary Datasets 1 and 2, respectively. The biomass equation was based on experimental measurements of the amino acid composition obtained from *K. stuttgartiensis* biomass pellets (Supplementary Table 1). Pseudofluxes were added to the model for specific metabolites to account for inactive metabolite pools that did not participate in metabolism, but contributed to measured metabolite labelling

patterns, similar to Ma et al. (2014)[50]. Chi-squared statistical tests were performed on resulting flux distributions to assess goodness-of-fit, and accurate 95% confidence intervals were computed for all estimated parameters by evaluating the sensitivity of the sum-of-squared residuals to parameter variations[51].

Amino acid composition analysis

Cultures were centrifuged (10,000 rpm, 15 mins, 4°C) to obtain cell pellets, which were subsequently freeze-dried prior to analysis. Total protein concentration was determined using the Pierce™ BCA Protein Assay Kit (ThermoFisher Scientific) and amino acid composition was determined according to Carnicer et al. (2009)[52] using a Varian 920-LC high performance liquid chromatography amino acid analyzer.

^{13}C protein stable isotope probing

Proteins were extracted from bioreactor cell pellets using glass bead beating (acid, washed, 0.1 mm diameter) in a suspension containing B-PER reagent (Thermo Scientific, Germany) and TEAB buffer (50 mM TEAB, 1% (w/w) NaDOC at pH 8). Following DTT reduction and alkylation using iodo acetamide (IAA) protein extracts were subject to proteolytic digestion using trypsin. Resulitng peptides were solid phase extraction purified using an Oasis HLB 96 well plate (Waters, UK), according to the manufacturer protocols. The purified peptide fraction was analysed via an one-dimensional reverse phase separtaion (Acclaim PepMap RSLC RP C18, 50 µm x 150 mm, 2µm, 100A) coupled to a Q-Exactive plus Orbitrap mass spectrometer (Thermo Scientific, Germany) operating in data depenedent aquision mode (DDA, shot-gun proteomics). The flow rate was maintained at 300 nL/min over a linear gradient from 5% to 30% over 90 minutes and finally to 75% B over 25 minutes. Solvent A was H_2O containing 0.1% formic acid, and solvent B consisted of 80% acetonitrile in H_2O and 0.1% formic acid. The Orbitrap was operated in DDA mode acquiring peptide signals form 350-1400 m/z, where the top 10 signals (with a charge between 2-7) were isolated at a window of 2.0 m/z and fragmented using a NCE of 30. The AGC target was set to 1e5, at a max IT of 54 ms and 17.5 K resolution. Protein identification and relative isotope abundances were determined from Tandem-MS data using PEAKS Studio X (BSI, Canada) and MetaProSIP (OpenMS, Univ Tuebingen/Berlin, Germany)[53] integrated into the KNIME 4.0.1 analysits platform (Zurich, Switzerland), respectively. All peptide spectra wer

matached against a protein database generated from predicted open reading frames from the *K. stuttgartiensis* genome.

Acknowledgements

The authors would like to acknowledge Patricia van Dam and Carol de Ram for help with metaproteomic sample preparation, Kathinka van de Pas-Schoonen for help with bioreactor maintenance, Paul van der Ven and Sebastian Kroose for help with amino acid analysis, and Arjan Pol and Huub Op den Camp for helpful discucssions. Funding was provided by the National Science Foundation (CBET-1435661, CBET-1803055 and MCB-1518130), the Netherlands Organization for Scientific Research (Grants 016.Vidi.189.050 and SIAM Gravitation Grant 024.002.002), the European Research Council (ERC Advanced Grant Ecomom 339880), a Wisconsin Distinguished Graduate Fellowship, a Postgraduate Scholarship-Doctoral (PGS-D) by the National Sciences and Engineering Research Council of Canada (NSERC), and the UW-Madison Office of the Vice Chancellor for Research and Graduate Education through the Microbiome Initiative.

Figure Legends

Figure 1. ^{13}C-enrichment of selected metabolites during ^{13}C-bicarbonate dynamic tracing experiments. (A) Mass isotopomer distributions (MID) for selected metabolites illustrating potential substrate channeling through the Wood-Ljungdahl Pathway and PFOR. (B) ^{13}C enrichment of metabolites associated with (left) initial CO_2 fixation reactions (Wood-Ljungdahl Pathway, pyruvate:ferredoxin oxidoreductase) and metabolites downstream of pyruvate; (center) TCA cycle metabolites; (right) gluconeogenesis and pentose phosphate pathway metabolites. (C) Selected mass isotopomer distributions for metabolites of the TCA cycle, gluconeogenesis, and the pentose phosphate pathway. All measured metabolite MIDs and standard errors can be found in Supplementary Dataset 1.

Figure 2. Elucidating TCA cycle of *K. stuttgartiensis* with ^{13}C-formate. (A) Proposed labelling of TCA cycle metabolites with ^{13}C-formate. (B) ^{13}C-enrichment of selected metabolites during isotope tracer experiments with ^{13}C-formate. (C) Time-series mass isotopomer distributions of

selected TCA cycle metabolites during isotope tracer experiments with ^{13}C-formate. All measured metabolite MIDs and standard errors can be found in Supplementary Dataset 1.

Figure 3. Operation of gluconeogenesis and pentose phosphate pathway in *K. stuttgartiensis* revealed by ^{13}C-formate dynamic labelling experiments. (A) proposed atom mapping of gluconeogenesis and pentose phosphate pathway from ^{13}C-formate labelled phosphoenolpyruvate at steady-state. (B) Time-series mass isotopomer distributions of selected gluconeogenesis and pentose phosphate pathway metabolites during dynamic isotope tracer experiments with ^{13}C-formate. All measured metabolite MIDs and standard errors can be found in Supplementary Dataset 1.

Figure 4. Reverse Wood-Ljungdahl pathway oxidizes acetate in *K. stuttgartiensis*. (A) Proposed labelling of TCA cycle metabolites with [2-^{13}C]acetate. (B) ^{13}C-enrichment of selected metabolites during isotope tracer experiments with [2-^{13}C]acetate (red). (C) Time-series mass isotopomer distributions of selected TCA cycle metabolites during isotope tracer experiments with ^{13}C-acetate. All measured metabolite MIDs and standard errors can be found in Supplementary Dataset 1.

Figure 5. *K. stuttgartiensis* flux map generated by ^{13}C INST-MFA. *K. stuttgartiensis* flux map under anaerobic, continuous flow, ammonium and nitrite medium conditions determined by fitting metabolites labelled with ^{13}C-formate tracers to a single, statistically acceptable isotopomer network model. Flux values represent the net flux through a given reaction +/- standard error defined at 95% confidence. All fluxes are normalized to a net CO_2 uptake rate of q=100 mmol-C/gDW/hr (actual CO_2 uptake rate was 0.186 mmol-C/gDW/hr). All isotopomer network model reactions are provided in Supplementary Dataset 2. INST-MFA solutions are provided in Supplementary Dataset 3.

Supplementary Figure 1. Confirmation of amino acid biosynthetic pathways in *K. stuttgartiensis*. (Right) Expected metabolite labeling patterns from ^{13}C-formate. (Left) Mass isotopomer distributions for measured intracellular amino acids.

Supplementary Figure 2. Confirmation of ^{13}C-labelled substrate incorporation into the proteome of *K. stuttgartiensis.* Distribution of relative isotope abundances for identified peptides assigned to the *K. stuttgartiensis* proteome during [2-^{13}C]acetate, ^{13}C-formate, and ^{13}C-bicarbonate tracer experiments after 0 and 72 hours.

Supplementary Figure 3. Proposed synthesis of sugar phosphates from gluconeogenesis and the RuMP cycle in *K. stuttgartiensis.* RuMP cycle reactions that synthesize fructose 6-phosphate (F6P) from formaldehyde (CH_2O) and ribulose 5-phosphate (Ru5P) are shown in orange. Production of CH_2O from formate via an unknown formaldehyde dehydrogenase is also show in orange. Reducing equivalents shown in pink; ATP shown in green; CO_2 shown in blue. *fdh*: formaldehyde dehydrogenase; *hps*: hexulose 6-phosphate synthase; *hpi*: hexulose 6-phosphate isomerase; *?* indicates no gene annotation present.

Supplementary Table 1. *K. stuttgartiensis* biomass amino acid composition.

Supplementary Dataset 1. Average metabolite mass isotopomer distributions and associated standard errors during ^{13}C-bicarbonate, ^{13}C-formate, and [2-^{13}C]acetate tracer experiments. (Sheet 1A) Average mass isotopomer distributions for selected metabolites during 13C-bicarbonate tracing, (Sheet 1B) Mass isotopomer distributions standard error values for selected metabolites during 13C-bicarbonate tracing, (Sheet 2A) Average mass isotopomer distributions for selected metabolites during 13C-formate tracing, (Sheet 2B) Mass isotopomer distributions standard error values for selected metabolites during 13C-formate tracing, (Sheet 3A) Average mass isotopomer distributions for selected metabolites during [2-13C]acetate tracing, (Sheet 3B) Mass isotopomer distributions standard error values for selected metabolites during [2-13C]acetate tracing.

Supplementary Dataset 2. *K. stuttgartiensis* isotopomer network model. Letters within brackets indicate carbon atom transitions of each metabolite for a given reaction.

Supplementary Dataset 3. INST-MFA model results. Metabolite MIDs used for model fitting were Pro, Asn, Ala, Thr, aKG, Ser, Suc, Asp, Glu, R5P, PEP, Cit, Mal, Ru5P, Fum, F6P, Pyr, G6P,

Val, CO2, and Gln at timepoints 0, 1.5, 3, 5, 8, 11, 15, 20, 30, and 45 minutes. All metabolite MIDs can be found in Supplementary Dataset 1.

Reference

1. Strous, M. *et al.* Missing lithotroph identified as new planctomycete. *Nature* **400**, 446–449 (1999).
2. Strous, M. *et al.* Deciphering the evolution and metabolism of an anammox bacterium from a community genome. *Nature* **440**, 790–4 (2006).
3. Kartal, B. *et al.* Molecular mechanism of anaerobic ammonium oxidation. *Nature* **479**, 127–30 (2011).
4. Kartal, B. *et al.* How to make a living from anaerobic ammonium oxidation. *FEMS Microbiol. Rev.* **37**, 428–461 (2013).
5. Jetten, M. S. M., Horn, S. J. & van Loosdrecht, M. C. M. Towards a more sustainable municipal wastewater treatment system. *Water Sci. Technol.* **35**, 171–180 (1997).
6. Kartal, B., Kuenen, J. G. & van Loosdrecht, M. C. M. Sewage Treatment with Anammox. *Science (80-.).* **328**, 702–703 (2010).
7. Lackner, S. *et al.* Full-scale partial nitritation/anammox experiences – An application survey. *Water Res.* **55**, 292–303 (2014).
8. Kartal, B. *et al.* Anammox bacteria disguised as denitrifiers: nitrate reduction to dinitrogen gas via nitrite and ammonium. *Environ. Microbiol.* **9**, 635–42 (2007).
9. Oshiki, M., Ali, M., Shinyako-Hata, K., Satoh, H. & Okabe, S. Hydroxylamine-dependent Anaerobic Ammonium Oxidation (Anammox) by " Candidatus Brocadia sinica". *Environ. Microbiol.* (2016). doi:10.1111/1462-2920.13355
10. Hu, Z., Wessels, H. J. C. T., van Alen, T., Jetten, M. S. M. & Kartal, B. Nitric oxide-dependent anaerobic ammonium oxidation. *Nat. Commun.* **10**, 1244 (2019).
11. van Niftrik, L. & Jetten, M. S. M. Anaerobic Ammonium-Oxidizing Bacteria: Unique Microorganisms with Exceptional Properties. *Microbiol. Mol. Biol. Rev.* **76**, 585 LP – 596 (2012).
12. Neumann, S. *et al.* Isolation and characterization of a prokaryotic cell organelle from the anammox bacterium Kuenenia stuttgartiensis. *Mol. Microbiol.* **94**, 794–802 (2014).
13. Almeida, N. M. De *et al.* Membrane-bound electron transport systems of an anammox

bacterium : A complexome analysis. *BBA - Bioenerg.* **1857**, 1694–1704 (2016).

14. Güven, D. *et al.* Propionate Oxidation by and Methanol Inhibition of Anaerobic Ammonium-Oxidizing Bacteria. *Appl. Environ. Microbiol.* **71**, 1066 LP – 1071 (2005).

15. Kartal, B. *et al.* Candidatus 'Anammoxoglobus propionicus' a new propionate oxidizing species of anaerobic ammonium oxidizing bacteria. *Syst. Appl. Microbiol.* **30**, 39–49 (2007).

16. Kartal, B. *et al.* Candidatus 'Brocadia fulgida': An autofluorescent anaerobic ammonium oxidizing bacterium. *FEMS Microbiol. Ecol.* **63**, 46–55 (2008).

17. Narita, Y. *et al.* Enrichment and physiological characterization of an anaerobic ammonium-oxidizing bacterium 'Candidatus Brocadia sapporoensis'. *Syst. Appl. Microbiol.* **40**, 448–457 (2017).

18. Schouten, S. *et al.* Stable Carbon Isotopic Fractionations Associated with Inorganic Carbon Fixation by Anaerobic Ammonium-Oxidizing Bacteria. *Appl. Environ. Microbiol.* **70**, 3785–3788 (2004).

19. Ali, M. *et al.* Physiological characterization of anaerobic ammonium oxidizing bacterium 'Candidatus Jettenia caeni'. *Environ. Microbiol.* **17**, 2172–2189 (2015).

20. Sweetlove, L. J. & Fernie, A. R. substrate channelling in metabolic regulation. *Nat. Commun.* **9**, 2136 (2018).

21. Ragsdale, S. W. & Pierce, E. Acetogenesis and the Wood – Ljungdahl pathway of CO2 fixation. *Biochim. Biophys. Acta* **1784**, 1873–1898 (2008).

22. Fuchs, G. Alternative Pathways of Carbon Dioxide Fixation : Insights into the Early Evolution of Life ? *Annu. Rev. Microbiol.* **65**, 631–658 (2011).

23. Lieber, D. J. *et al.* A multienzyme complex channels substrates and electrons through acetyl-CoA and methane biosynthesis pathways in Methanosarcina. *PLoS One* **9**, e107563–e107563 (2014).

24. Meyer, P., Cecchi, G. & Stolovitzky, G. Spatial localization of the first and last enzymes effectively connects active metabolic pathways in bacteria. *BMC Syst. Biol.* **8**, 131 (2014).

25. Howell, D. M., Xu, H. & White, R. H. (R)-Citramalate Synthase in Methanogenic Archaea. *J. Bacteriol.* **181**, 331 LP – 333 (1999).

26. Li, F., Hagemeier, C. H., Seedorf, H., Gottschalk, G. & Thauer, R. K. Re -Citrate Synthase from Clostridium kluyveri Is Phylogenetically Related to Homocitrate Synthase

and Isopropylmalate Synthase Rather Than to Si -Citrate Synthase. *J. Bacteriol.* **189**, 4299–4304 (2007).

27. Risso, C., Dien, S. J. Van, Orloff, A., Lovley, D. R. & Coppi, M. V. Elucidation of an Alternate Isoleucine Biosynthesis Pathway in Geobacter sulfurreducens. *J. Bacteriol.* **190**, 2266–2274 (2008).

28. Tang, Y. J. *et al.* Investigation of Carbon Metabolism in Dehalococcoides ethenogenes Strain 195 by Use of Isotopomer and Transcriptomic Analyses. *J. Bacteriol.* **191**, 5224 LP – 5231 (2009).

29. Oshiki, M., Shimokawa, M., Fujii, N., Satoh, H. & Okabe, S. Physiological characteristics of the anaerobic ammonium-oxidizing bacterium ‘ Candidatus Brocadia sinica ’. *Microbiology* **157**, 1706–1713 (2011).

30. Russ, L. *et al.* Genome analysis and heterologous expression of acetate-activating enzymes in the anammox bacterium Kuenenia stuttgartiensis. *Arch. Microbiol.* **194**, 943–948 (2012).

31. Spormann, A. M. & Thauer, R. K. Anaerobic acetate oxidation to CO2 by Desulfotomaculum acetoxidans. *Arch. Microbiol.* **150**, 374–380 (1988).

32. Schauder, R., Preu, A., Jetten, M. & Fuchs, G. Oxidative and reductive acetyl CoA/carbon monoxide dehydrogenase pathway in Desulfobacterium autotrophicum. *Arch. Microbiol.* **151**, 84–89 (1989).

33. Mayer, F. *et al.* AMP-Forming Acetyl Coenzyme A Synthetase in the Outermost Membrane of the Hyperthermophilic Crenarchaeon Ignicoccus hospitalis. *J. Bacteriol.* **194**, 1572 LP – 1581 (2012).

34. Young, J. D., Walther, J. L., Antoniewicz, M. R., Yoo, H. & Stephanopoulos, G. An elementary metabolite unit (EMU) based method of isotopically nonstationary flux analysis. *Biotechnol. Bioeng.* **99**, 686–99 (2008).

35. Kato, N., Yurimoto, H. & Thauer, R. K. The Physiological Role of the Ribulose Monophosphate Pathway in Bacteria and Archaea. *Biosci. Biotechnol. Biochem.* **70**, 10–21 (2006).

36. W, F. P., Williams, T. C. R., Sweetlove, L. J. & Ratcliffe, R. G. Capturing Metabolite Channeling in Metabolic. *Plant Physiol.* **157**, 981–984 (2011).

37. Bulutoglu, B., Garcia, K. E., Wu, F., Minteer, S. D. & Banta, S. Direct Evidence for

Metabolon Formation and Substrate Channeling in Recombinant TCA Cycle Enzymes. *ACS Chem. Biol.* (2016). doi:10.1021/acschembio.6b00523

38. Speth, D. R., in ’t Zandt, M. H., Guerrero-Cruz, S., Dutilh, B. E. & Jetten, M. S. M. Genome-based microbial ecology of anammox granules in a full-scale wastewater treatment system. *Nat. Commun.* **7**, 11172 (2016).

39. Lawson, C. E. *et al.* Metabolic network analysis reveals microbial community interactions in anammox granules. *Nat. Commun.* **8**, 1–12 (2017).

40. Winkler, M. K. H. *et al.* Nitrate reduction by organotrophic Anammox bacteria in a nitritation / anammox granular sludge and a moving bed biofilm reactor. *Bioresour. Technol.* **114**, 217–223 (2012).

41. Le, T. *et al.* Nitrate residual as a key parameter to efficiently control partial denitrification coupling with anammox. *Water Environ. Res.* 1–11 (2019). doi:10.1002/wer.1140

42. Mellbye, B. L. *et al.* Genome-Scale, Constraint-Based Modeling of Nitrogen Oxide Fluxes during Coculture of Nitrosomonas europaea and Nitrobacter winogradskyi. *mSystems* **3**, e00170-17 (2018).

43. Graaf, A. A. Van De, Bruijn, P. De, Robertson, L. A., Jetten, M. M. & Kuenen, J. G. Autotrophic growth of anaerobic ammonium-oxidzing micro-organisms in a fluidized bed reactor. *Microbiology* **142**, 2187–96 (1996).

44. Su, X., Lu, W. & Rabinowitz, J. D. Metabolite Spectral Accuracy on Orbitraps. *Anal. Chem.* **89**, 5940–5948 (2017).

45. Yang, W.-C. *et al.* Simultaneous Quantification of Metabolites Involved in Central Carbon and Energy Metabolism Using Reversed-Phase Liquid Chromatography−Mass Spectrometry and in Vitro 13C Labeling. *Anal. Chem.* **80**, 9508–9516 (2008).

46. Jannasch, A., Sedlak, M. & Adamec, J. Quantification of Pentose Phosphate Pathway (PPP) Metabolites by Liquid Chromatography-Mass Spectrometry (LC-MS) BT - Metabolic Profiling: Methods and Protocols. in (ed. Metz, T. O.) 159–171 (Humana Press, 2011). doi:10.1007/978-1-61737-985-7_9

47. Kamphorst, J. J. *et al.* Human Pancreatic Cancer Tumors Are Nutrient Poor and Tumor Cells Actively Scavenge Extracellular Protein. **75**, 544–554 (2015).

48. Åberg, J. & Wallin, B. Evaluating a fast headspace method for measuring DIC and subsequent calculation of pCO2 in freshwater systems. *Inl. Waters* **4**, 157–166 (2014).

49. Young, J. D. INCA : a computational platform for isotopically non-stationary metabolic flux analysis. *Bioinformatics* **30**, 1333–1335 (2014).
50. Ma, F., Jazmin, L. J., Young, J. D. & Allen, D. K. Isotopically nonstationary 13C flux analysis of changes in Arabidopsis thaliana leaf metabolism due to high light acclimation. *Proc. Natl. Acad. Sci.* **111**, 16967 LP – 16972 (2014).
51. Antoniewicz, M. R., Kelleher, J. K. & Stephanopoulos, G. Determination of confidence intervals of metabolic fluxes estimated from stable isotope measurements. *Metab. Eng.* **8**, 324–337 (2006).
52. Carnicer, M. *et al.* Macromolecular and elemental composition analysis and extracellular metabolite balances of Pichia pastoris growing at different oxygen levels. *Microb. Cell Fact.* **8**, 65 (2009).
53. Sachsenberg, T. *et al.* MetaProSIP: Automated Inference of Stable Isotope Incorporation Rates in Proteins for Functional Metaproteomics. *J. Proteome Res.* **14**, 619–627 (2015).

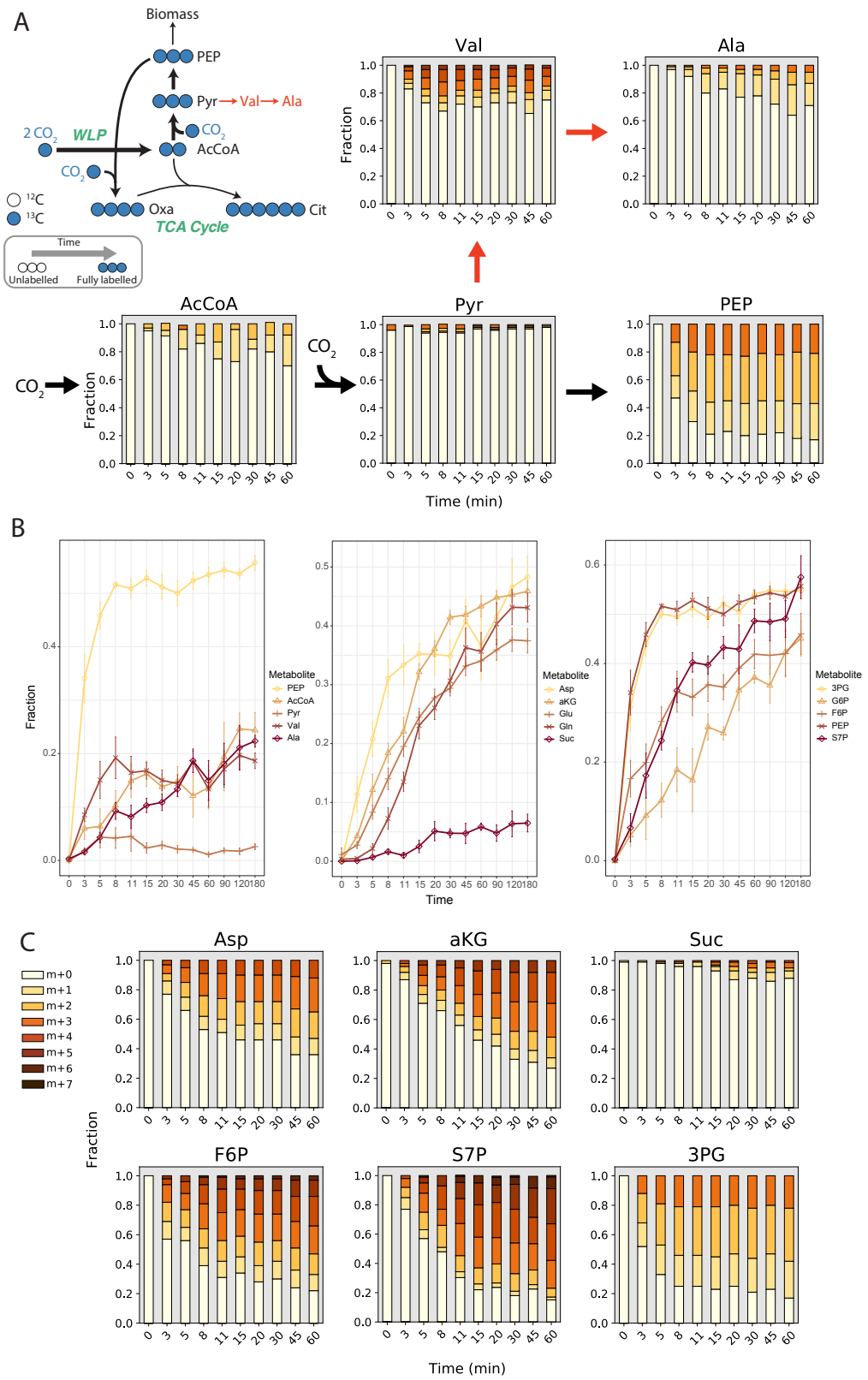

Figure 1. ^{13}C-enrichment of selected metabolites during ^{13}C-bicarbonate dynamic tracing experiments.

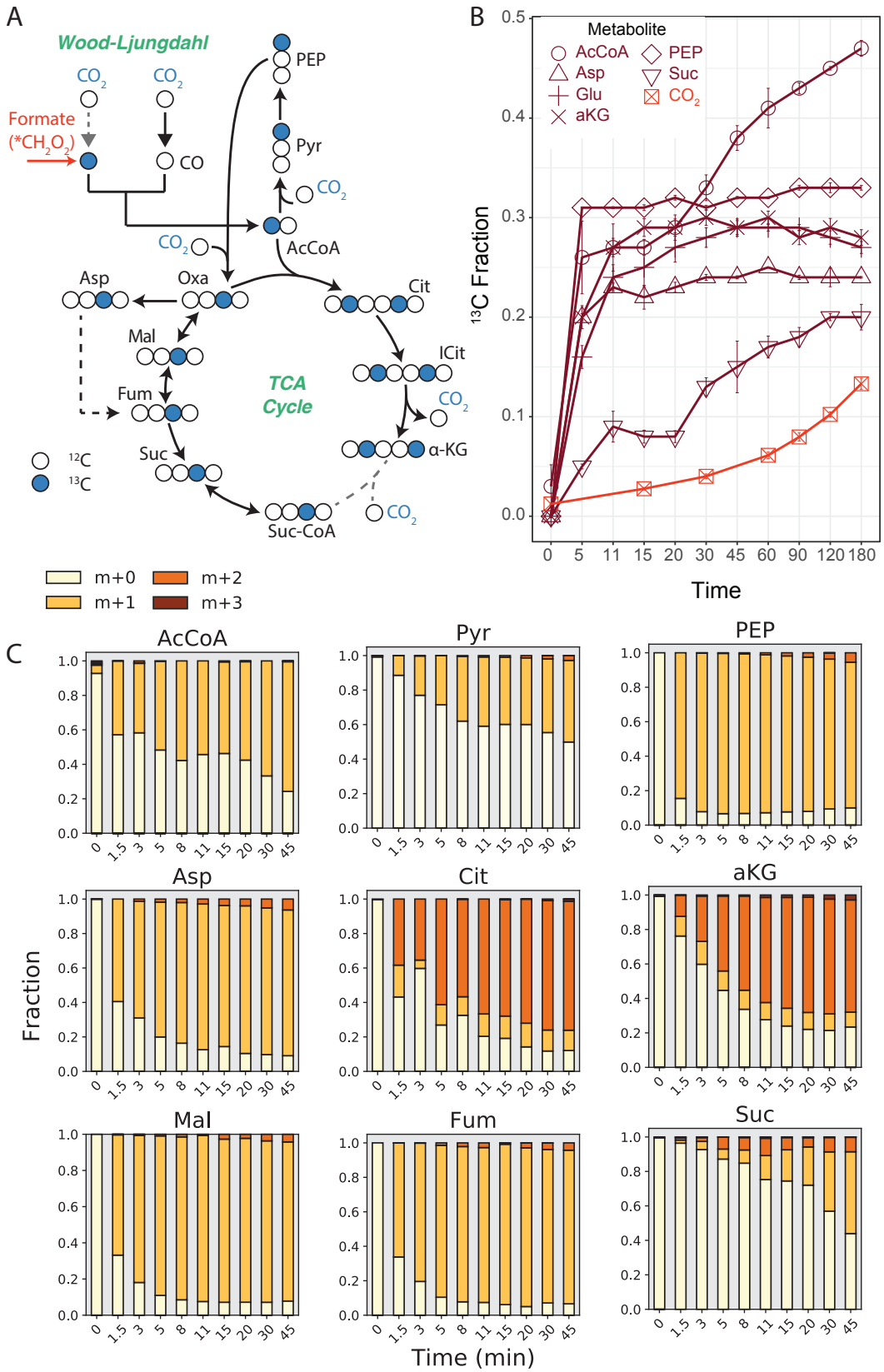

Figure 2. Elucidating TCA cycle of *K. stuttgartiensis* with ^{13}C-formate.

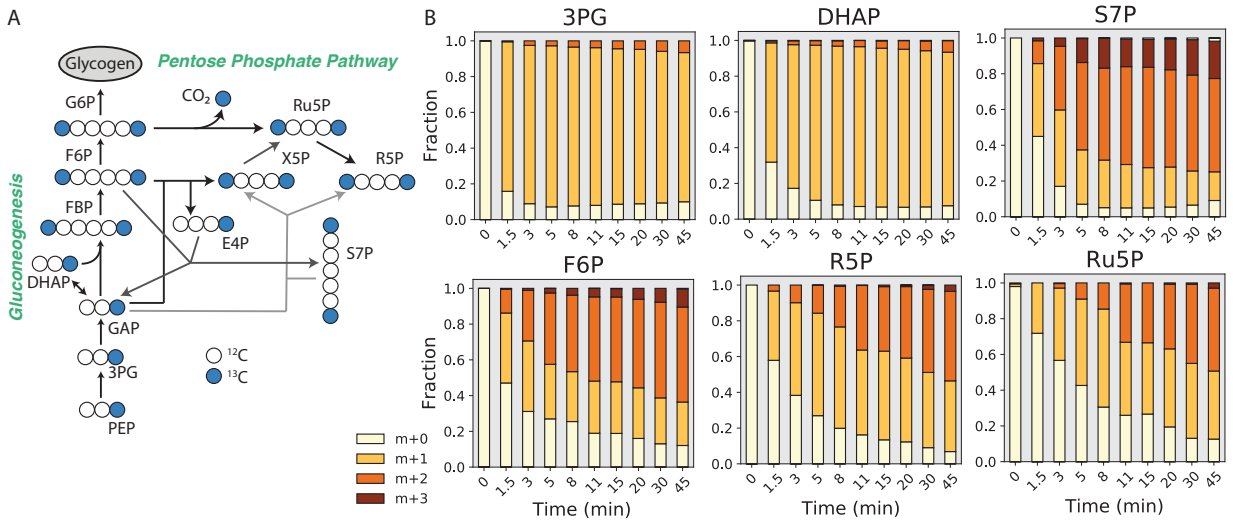

Figure 3. Operation of gluconeogenesis and pentose phosphate pathway in *K. stuttgartiensis* revealed by ^{13}C-formate dynamic labelling experiments.

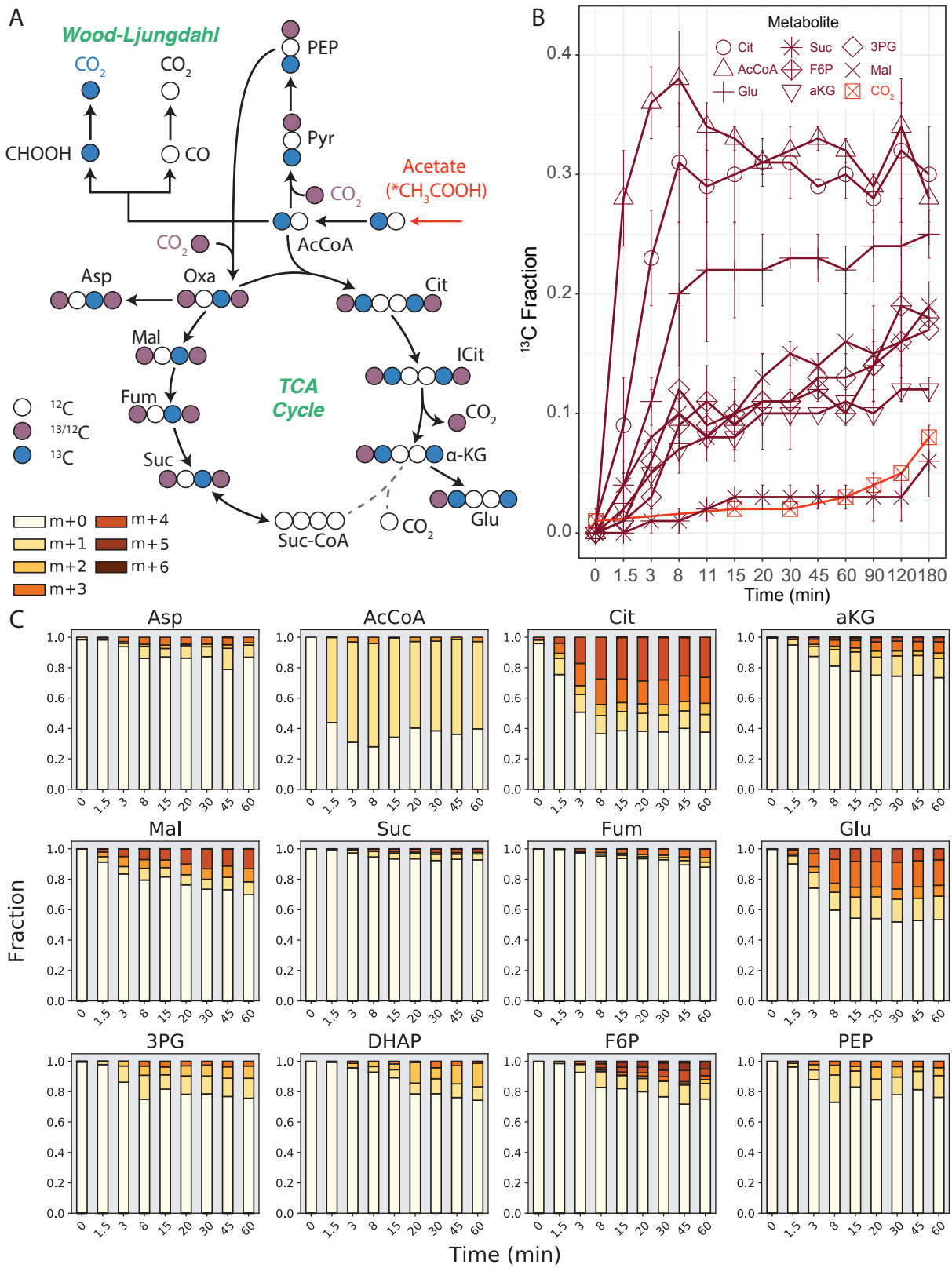

Figure 4. Reverse Wood-Ljungdahl pathway oxidizes acetate in *K. stuttgartiensis*.

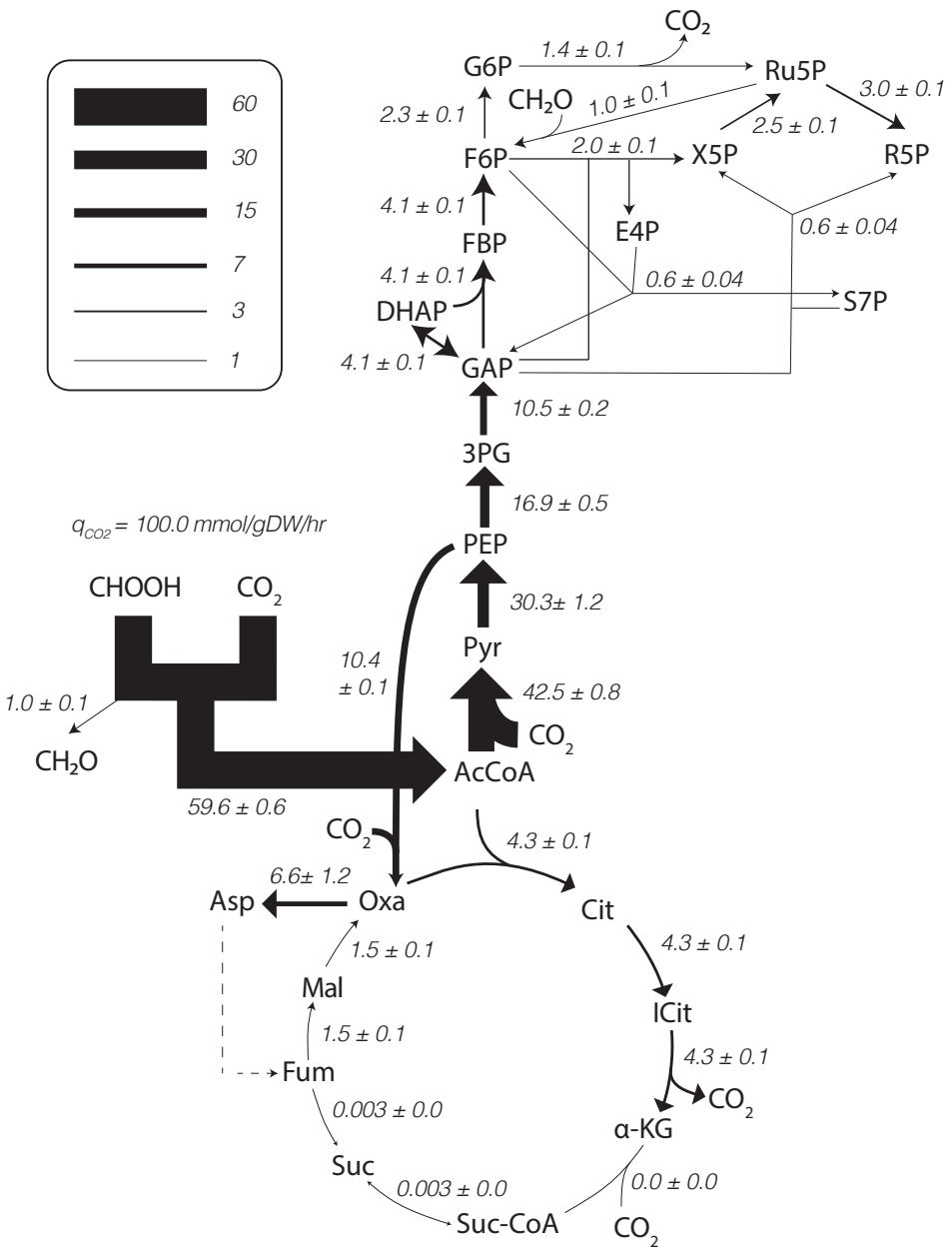

Figure 5. *K. stuttgartiensis* flux map generated by ^{13}C INST-MFA.

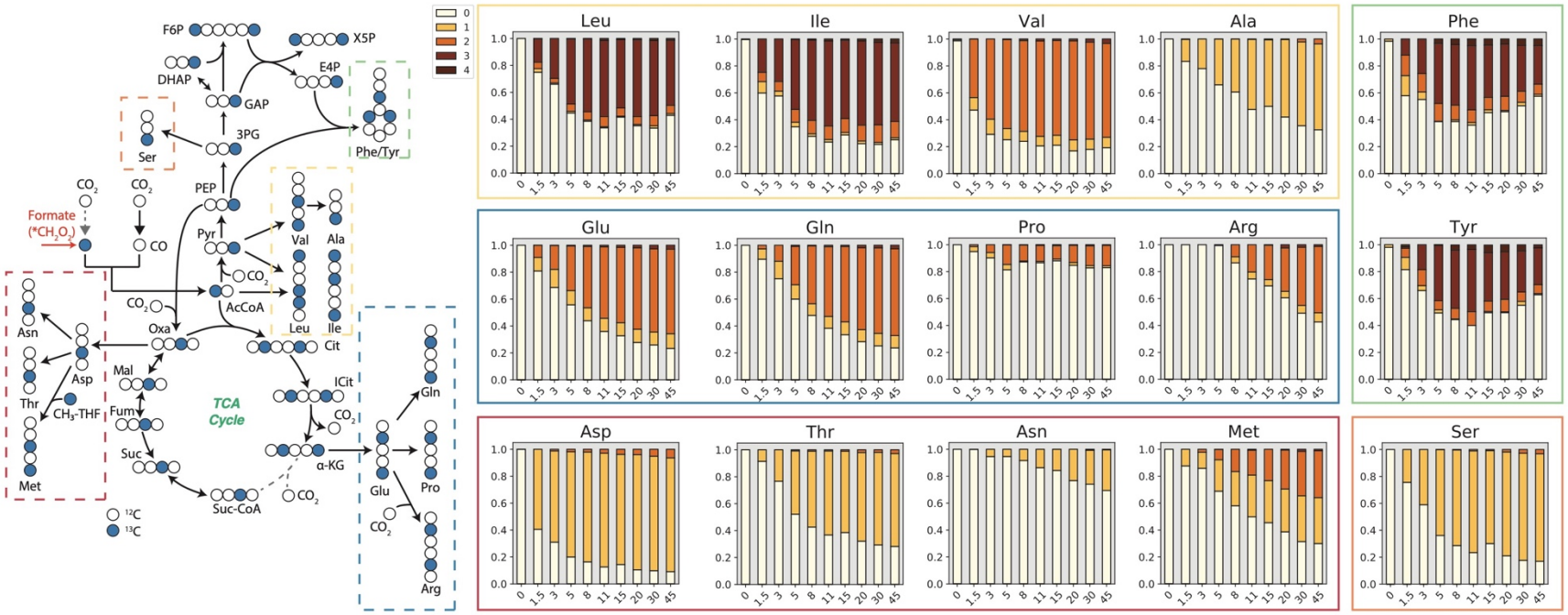

Supplementary Figure 1. Confirmation of amino acid biosynthetic pathways in *K. stuttgartiensis*.

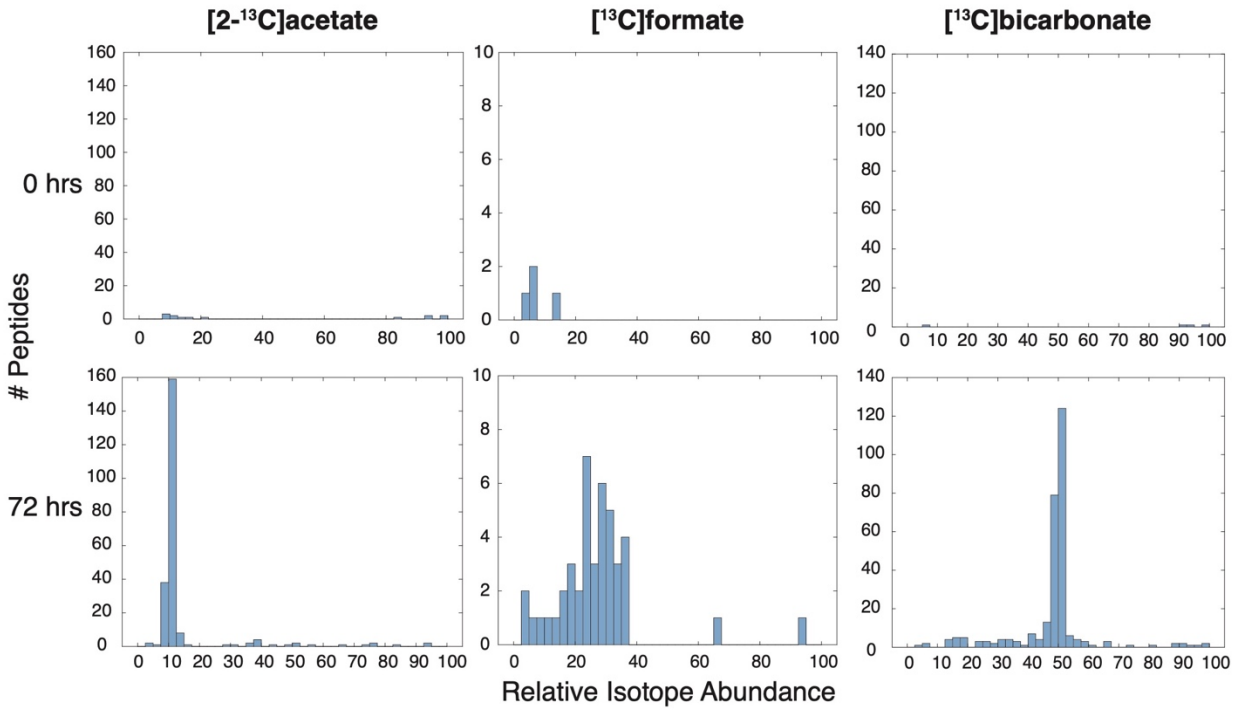

Supplementary Figure 2. Confirmation of ^{13}C-labelled substrate incorporation into the proteome of *K. stuttgartiensis.*

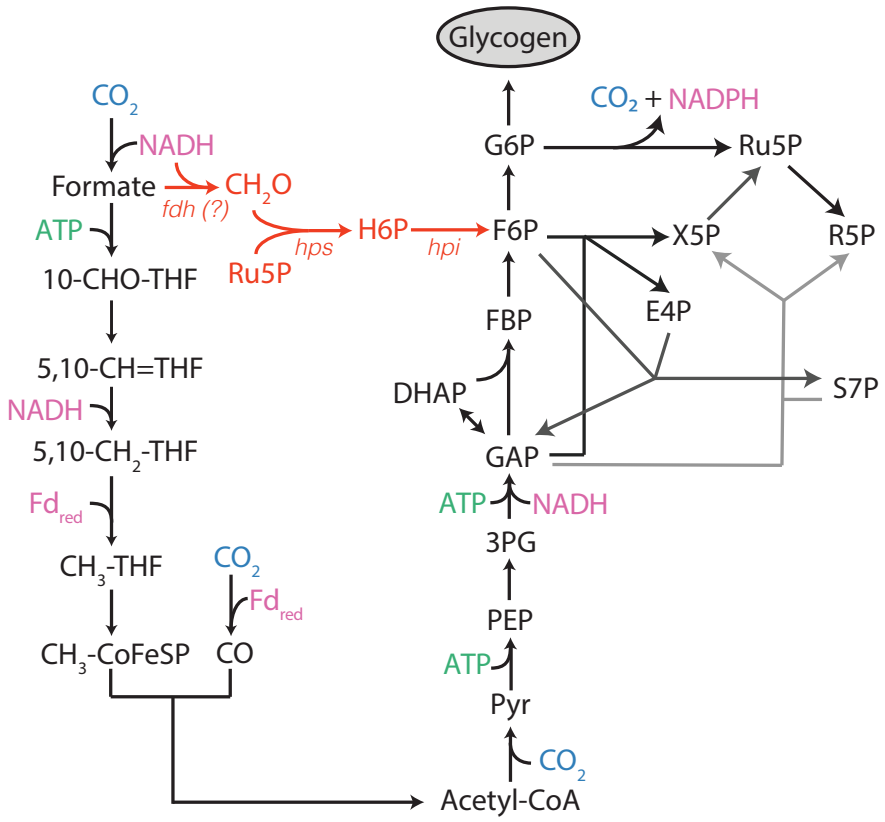

Supplementary Figure 3. Proposed synthesis of sugar phosphates from gluconeogenesis and the RuMP cycle in *K. stuttgartiensis*.

Amino Acid	Mass (umol/mgDW)	Std Dev (umol/mgDW)
Ala	374.6	38.7
Arg	278.9	56.7
Asp	130.0	10.2
Glu	107.5	8.5
Gly	778.8	117.4
His	42.2	7.6
Ile	267.8	43.4
Leu	393.2	55.3
Lys	154.8	44.1
Met	218.9	58.4
Phe	205.4	43.0
Pro	460.0	96.1
Ser	436.5	94.1
Thr	381.0	86.5
Val	438.2	76.2

Supplementary Table 1. *K. stuttgartiensis* biomass amino acid composition.